



ELSEVIER

Available online at [www.sciencedirect.com](http://www.sciencedirect.com)

Journal of Volcanology and Geothermal Research 170 (2008) 99–110

---



---

 Journal of volcanology  
and geothermal research
 

---



---

[www.elsevier.com/locate/jvolgeores](http://www.elsevier.com/locate/jvolgeores)

## Evaluation of ASTER and SRTM DEM data for lahar modeling: A case study on lahars from Popocatépetl Volcano, Mexico

C. Huggel<sup>a,\*</sup>, D. Schneider<sup>a</sup>, P. Julio Miranda<sup>b</sup>, H. Delgado Granados<sup>b</sup>, A. Kääh<sup>c</sup>

<sup>a</sup> *Glaciology and Geomorphodynamics Group, Department of Geography, University of Zurich, Winterthurerstr. 190, 8057 Zurich, Switzerland*

<sup>b</sup> *Instituto de Geofísica, Universidad Nacional Autónoma de México, C.U., Coyoacán, 04510, México D.F., México*

<sup>c</sup> *Department of Geoscience, University of Oslo, Norway*

Received 6 September 2007

Available online 19 September 2007

### Abstract

Lahars are among the most serious and far-reaching volcanic hazards. In regions with potential interactions of lahars with populated areas and human structures the assessment of the related hazards is crucial for undertaking appropriate mitigating actions and reduce the associated risks. Modeling of lahars has become an important tool in such assessments, in particular where the geologic record of past events is insufficient. Mass-flow modeling strongly relies on digital terrain data. Availability of digital elevation models (DEMs), however, is often limited and thus an obstacle to lahar modeling. Remote-sensing technology has now opened new perspectives in generating DEMs. In this study, we evaluate the feasibility of DEMs derived from the Advanced Spaceborne Thermal Emission and Reflection Radiometer (ASTER) and the Shuttle Radar Topography Mission (SRTM) for lahar modeling on Popocatépetl Volcano, Mexico. Two GIS-based models are used for lahar modeling, LAHARZ and a flow-routing-based debris-flow model (modified single-flow direction model, MSF), both predicting areas potentially affected by lahars. Results of the lahar modeling show that both the ASTER and SRTM DEMs are basically suitable for use with LAHARZ and MSF. Flow-path prediction is found to be more reliable with SRTM data, though with a coarser spatial resolution. Errors of the ASTER DEM affecting the prediction of flow paths due to the sensor geometry are associated with deeply incised gorges with north-facing slopes. LAHARZ is more sensitive to errors of the ASTER DEM than the MSF model. Lahar modeling with the ASTER DEM results in a more finely spaced predicted inundation area but does not add any significant information in comparison with the SRTM DEM. Lahars at Popocatépetl are modeled with volumes of  $1 \times 10^5$  to  $8 \times 10^6$  m<sup>3</sup> based on ice-melt scenarios of the glaciers on top of the volcano and data on recent and historical lahar events. As regards recently observed lahars, the travel distance of lahars of corresponding volume modeled with LAHARZ falls short by 2 to 4 km. An important finding is that the travel distance of potential lahar events modeled with LAHARZ may differ by about 2 km when using SRTM or ASTER data because of varying lateral flow-volume distribution. As a consequence, verification and sensitivity analysis of the DEM is fundamental to deriving hazard maps from predicted modeled inundation areas. Because of the global coverage of this type of remote-sensing data, the conclusion that both SRTM and ASTER-derived DEMs are feasible for lahar modeling opens a wide field of application in volcanic-hazards studies. © 2007 Elsevier B.V. All rights reserved.

**Keywords:** lahar modeling; LAHARZ; SRTM; ASTER; digital elevation model (DEM)

### 1. Introduction

Mass movements such as debris avalanches and lahars descending from volcanoes, directly or indirectly related to eruptive activity, are among the most serious and far-reaching volcanic hazards. Many volcanoes with potential lahar hazards endanger human settlements and their infrastructures. Modeling of lahars has become crucial for hazards assessment, in particular

in areas with inadequate knowledge of the geological record of past lahar events. The downslope propagation of lahars, like other volcanic mass movements, is strongly controlled by topography. Models simulating volcanic mass movements necessarily require as input a digital representation of the terrain. Digital elevation models (DEM), however, are of limited availability in many volcanic regions, especially for remote or less developed areas.

Space-borne earth-observation sensors provide new perspectives in DEM generation for virtually any location on earth. The Advanced Spaceborne Thermal Emission and Reflection Radiometer (ASTER) onboard the NASA Terra satellite has

\* Corresponding author. Tel.: +41 44 635 51 75; fax: +41 44 635 68 48.  
E-mail address: [chuggel@geo.unizh.ch](mailto:chuggel@geo.unizh.ch) (C. Huggel).

the capability of taking along-track stereo images allowing the generation of high-resolution DEMs (Kääb, 2002; Stevens et al., 2004; Kääb, 2005). The Shuttle Radar Topography Mission (SRTM) provides unique DEM data with 30 to 90 m resolution based on an InSAR campaign in February 2000 (Rabus et al., 2003). However, both ASTER and SRTM data have not yet been thoroughly exploited for mass movement modeling and related hazard assessments for volcanic regions.

The main objective of this paper is to evaluate the potential and limitations of SRTM and ASTER-derived DEM data for lahar modeling. To gain a more comprehensive perspective, two GIS-based lahar models are applied: the widely used LAHARZ developed by Iverson et al. (1998) and a debris-flow model presented by Huggel et al. (2003). To this end, a volcano with comprehensive and recent lahar studies and modeling was selected.

Popocatepetl Volcano is located in the Trans-Mexican Volcanic Belt, 40–60 km from large metropolitan areas such as Puebla, Cuernavaca, and Mexico City, and near several towns and villages with tens of thousands of inhabitants (Fig. 1). Popocatepetl Volcano has a fairly good geological record of past lahars (Delgado Granados et al., 1994, 1995; Siebe et al., 1996; González Huesca et al., 1997; Palacios et al., 1998; Siebe et al., 1999; González Huesca, 2000). Lahar hazards at Popocatepetl deserve additional attention due to the existence of glacier ice on top of the volcano and the possibility of eruption-induced ice-melt processes as lahar triggers (Delgado Granados and Brugman, 1995; Brugman and Delgado Granados, 1998; Palacios and Marcos, 1998; Julio Miranda and Delgado Granados, 2003; Bursik et al., 2003). Lahars are in fact one of the major hazards of glacier-clad volcanoes (Major and Newhall, 1989; Thouret, 1990). The glaciers of Popocatepetl experienced a strong retreat

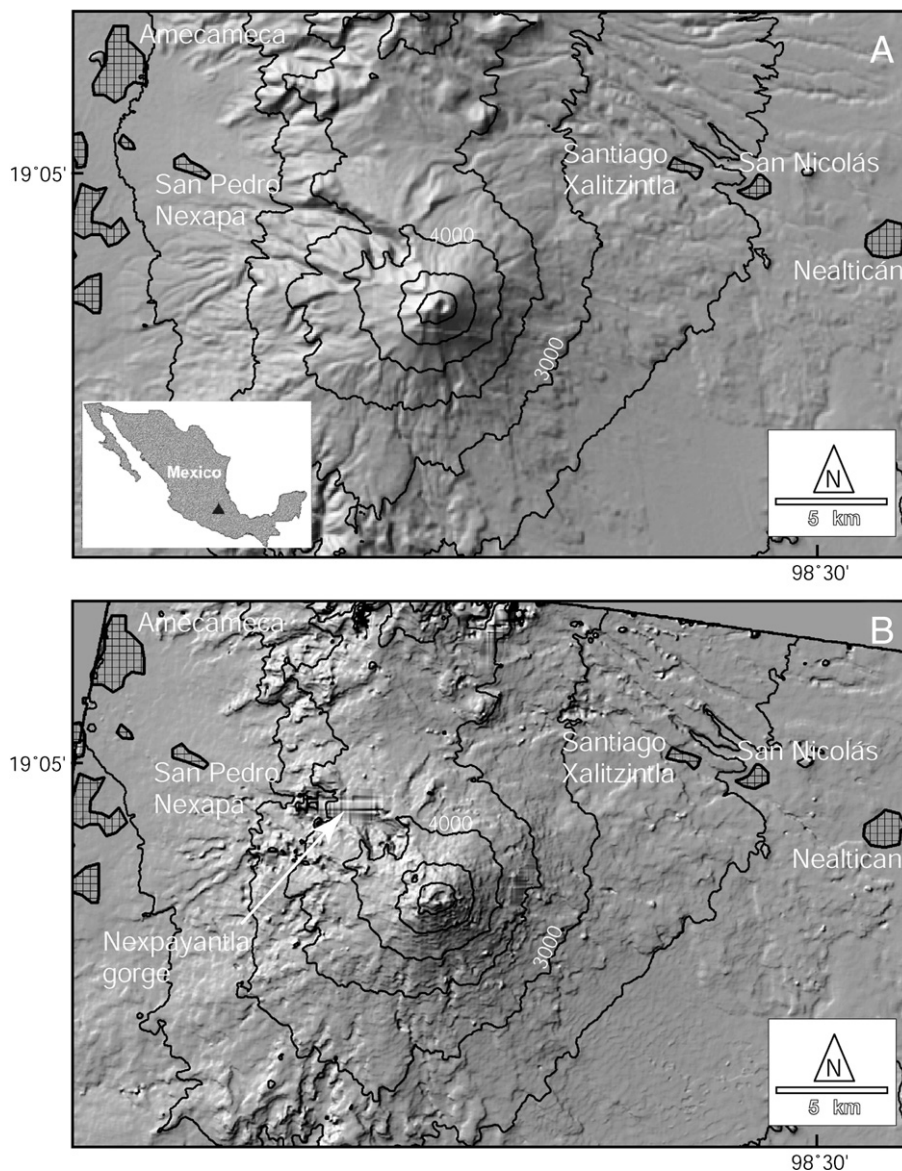


Fig. 1. Location of Popocatepetl Volcano in central Mexico (inset). Shaded SRTM (A) and ASTER (B) DEMs of the Popocatepetl Volcano area are shown. Contour lines are at 500 m interval. The most important villages and towns, relevant for lahar modeling studies are indicated. Note the erroneous area in the ASTER DEM at the Nexpayantla gorge.

in recent years, accelerated by the eruptive activity (Delgado Granados, 1997; Huggel and Delgado, 2000; Julio Miranda and Delgado Granados, 2003). A number of lahar events since volcanic activity resumed at Popocatepetl in 1994 were directly related to snow and ice melting of glaciers, and several lahars reached populated areas (González Huesca and Delgado Granados, 1997; Palacios et al., 2001; Bursik et al., 2003; Capra et al., 2004; Julio Miranda et al., 2005). The information available for such events enables realistic analysis of the modeled lahars.

It should be noted, however, that detailed assessment of lahar hazards around Popocatepetl is not the primary objective of this study. Rather, we strive to evaluate the degree of success of lahar models using SRTM and ASTER DEM data before they are applied in regions for which DEM data are not available.

## 2. Remote sensing-derived DEM data

### 2.1. Shuttle Radar Topography Mission (SRTM)

SRTM was a single pass, synthetic aperture radar interferometry (InSAR) campaign conducted in February 2000. For the first time a global high-quality DEM was achieved with a resolution of 1 arc sec ( $\sim 30$  m) and 3 arc sec ( $\sim 90$  m, free availability) covering the Earth's area between  $60^\circ\text{N}$  and  $54^\circ\text{S}$  (Van Zyl, 2001). Vertical errors of the DEM are  $\pm 16$  m and  $\pm 6$  m for absolute and relative accuracy, respectively; the horizontal positional accuracy is  $\pm 20$  m at a 90% confidence level (Rabus et al., 2003). Absolute accuracy thereby relates to the error throughout the entire mission while relative accuracy describes the error at a local 200 km-scale. First assessments in high-mountain terrain compared the 90 m SRTM DEM with aerophotogrammetric DEMs and found root mean square errors (RMSE) of the height of 12–36 m and maximum vertical errors of more than 100 m in extremely rough topography (Kääb, 2005). Other studies in relatively flat terrain reported an RMSE of SRTM DEM data of about 10 m in comparison with shuttle laser altimeter data (Sun et al., 2003). In mountainous terrain, the SRTM DEM shows sections with data gaps, generally due to radar shadow, layover and insufficient interferometric coherence (Kääb, 2005).

For this study, a  $30\text{ km} \times 40\text{ km}$  SRTM DEM was used and resampled at a grid resolution of 90 m. Only a few data gaps were present in this DEM subset and were of marginal relevance for the purpose of this study. The positional accuracy is within the subpixel range when compared with 1:50,000 topographic maps. Random tests of the vertical error of the SRTM data with reference to the 1:50,000 maps showed a similar absolute accuracy, in accordance with technical sensor specifications (Rabus et al., 2003). Fig. 1A shows a shaded terrain view of the SRTM DEM. Stream-flow channels are well represented and without any significant errors.

### 2.2. Advanced Spaceborne Thermal Emission and Reflection Radiometer (ASTER)

The ASTER sensor onboard the NASA Terra satellite provides imagery with visible and near-infrared (VNIR) bands in

15 m spatial resolution, and short-wave and thermal infrared bands with 30 m and 90 m resolution, respectively (Abrams, 2000). With these high-resolution multispectral capabilities, ASTER imagery has recently become a promising tool in detecting volcanic activity, applied, for instance, to volcanic cloud and gas analysis (Pieri and Abrams, 2004). DEM generation is facilitated by a 15 m along-track stereo-band looking  $27.6^\circ$  backwards from nadir. Terra has a repeat cycle of 16 days but given the ASTER swath width of 60 km and its 8% duty cycle, a stereo pair can be obtained approximately every 44 days (Stevens et al., 2004). However, in urgent cases such as natural disasters, the repeat period can be reduced to about 2 days, thanks to the  $\pm 8.5^\circ$  cross-track pointing capabilities of the ASTER sensor, with additional across-track viewing capabilities of up to  $\pm 24^\circ$  for the VNIR bands only (for a disaster-related example, cf. Kääb et al., 2003).

Here, an ASTER stereo image taken on 17 March 2001 covering the entire Popocatepetl Volcanic edifice was acquired. Generation of the DEM based on the stereo images was done with PCI Geomatica software using an algorithm developed by Toutin and Cheng (2001). Geo-correction of the ASTER image and DEM was achieved using ground control points extracted from the 1:50,000 topographic maps. The horizontal position accuracy of the DEM was 3 pixels (40–50 m). An evaluation of the ASTER DEM generated for the Popocatepetl area shows an overall satisfactory quality in spite of problems in areas of complex topography (Fig. 1B). Significant DEM errors were identified in the steeply incised Nexpayantla gorge, the main drainage towards the populated areas northwest of the volcano. The errors are likely related to the steep north-facing slopes of the gorge which imply an overly small incidence angle of the  $27.6^\circ$ -backlooking stereo sensor with the terrain surface, resulting in inconsistencies in the DEM generation process.

### 2.3. SRTM DEM vs. ASTER DEM

For vertical error quantification, the ASTER DEM was compared with the SRTM DEM (Fig. 2). For a  $15\text{ km} \times 30\text{ km}$  subset including the erroneous areas of the Nexpayantla gorge, the RMS of the vertical error relative to the SRTM DEM was 38 m with sporadic maximum errors of up to about 500 m. A  $10\text{ km} \times 10\text{ km}$  subset excluding the erroneous areas showed an RMSE of 27 m. These results are consistent with recent findings indicating an RMSE of the elevation difference between 15 and 70 m depending on topographic conditions (Kääb, 2002; Hirano et al., 2003; Stevens et al., 2004; Kääb, 2005). These error ranges refer to an ASTER DEM generated with 30 m resolution (2 image pixels). An ASTER DEM based on the same stereo imagery generated with 60 m resolution reduced the maximum height errors by about 200 m but the RMS error remained approximately the same. For the lahar modeling the 30 m ASTER DEM was used.

In general, the analysis of the SRTM and ASTER DEMs of Popocatepetl confirmed the conclusions of previous studies that the SRTM DEM shows less gross errors than the ASTER DEM, with maximum errors of the ASTER DEM several hundred meters larger than those of the SRTM DEM (Kääb, 2005). For



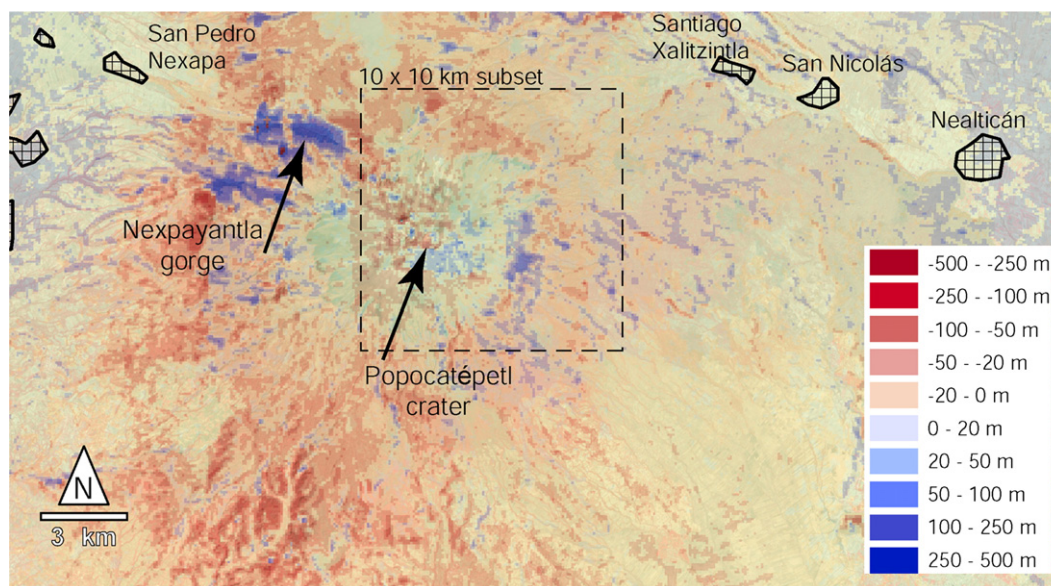


Fig. 2. Comparison of the ASTER DEM relative to the SRTM DEM. Negative (positive) values refer to lower (higher) elevations in the ASTER DEM relative to the SRTM DEM. The location of the  $10 \times 10$  km subset used for accuracy tests excluding the main erroneous area of the Nexpayantla gorge is indicated. Less-rugged terrain generally shows less deviations of the ASTER DEM from the SRTM DEM.

the subsequent modeling studies, the large height errors such as those at Nexpayantla gorge are relevant and may cause significant deviation of the simulated lahar-flow from the true drainage pathways.

### 3. Models for lahar flow-simulation

Both models applied here for lahar modeling are strongly topography-driven. Model integration in a GIS environment facilitates handling of remote-sensing-derived data. Hence, they are well suited for the evaluation of SRTM and ASTER-derived terrain data used for lahar modeling. Both models are flow-routing models based on topography and geometry without explicit hydraulic considerations. This may be a model limitation when detailed studies on a local scale are the objective. Here, however, our focus is on approximate delineation of lahar-endangered zones at a regional scale. Below, a brief description of the models is given for clarity.

#### 3.1. LAHARZ

LAHARZ is a widely used model to delineate potential lahar inundation zones and was developed by Iverson et al. (1998) and Schilling (1998). The model is a fast, automatic and objective tool for assessment of lahar-endangered areas based on the principles that: a) the lahar volume largely controls the extent of downstream inundation; b) past lahars provide a basis for future lahars; and c) large lahars occur less often than small ones (Iverson et al., 1998). The model uses standard ARC/INFO® functions to derive flow path and directions on an input DEM. Potential inundation zones are calculated based on an empirical relationship between lahar volume, and cross-sectional and planimetric area of inundation (Iverson et al., 1998). The channel or valley cross-section is filled to a level that satisfies the em-

pirical relationship. The onset of inundation and deposition is defined by distinguishing between proximal and distal hazard zones based on the energy-cone concept (Malin and Sheridan, 1982) using a ratio of vertical descent ( $H$ ) to horizontal runout ( $L$ ) from about 0.1 to 0.3. Main input data and variables for LAHARZ are a DEM, the defined  $H/L$  ratio, a drainage channel starting location, and the specified lahar volume. According to the principle that large lahars occur less often than small ones, different lahar volumes and the corresponding inundation zones represent the degree of hazard encountered.

#### 3.2. Modified single-flow direction model (MSF)

The modified single-flow direction (MSF) model applied here was developed by Huggel et al. (2003) for debris flow-type mass movements in high-mountain environments. The debris flow is considered as a downslope moving mass largely controlled by gravitational force and following a given topography. The model includes a trajectory component which calculates the potentially inundated areas, and a runout component which defines the runout distance of the debris flow.

##### 3.2.1. Trajectory and flow-routing component of model

Like LAHARZ, the MSF model is integrated in a GIS ARC/INFO® environment and uses the D8 flow-direction algorithm introduced by O'Callaghan and Mark (1984). The model principle implies a downslope propagation of a debris flow or lahar from a specified initiation point. The central flow line of the mass flow is assumed to follow the direction of steepest descent as calculated by the single-flow direction (D8) algorithm. To account for the lahar behavior implying flow spreading in flatter terrain, a flow diversion function  $F_d$  was incorporated into the model. This function allows the flow to divert from the direction of steepest descent up to  $45^\circ$  on both

sides. Thus, the model is better able to simulate the different characteristics of lahars in confined channel sections (with largely limited spread due to converging flow) and on relatively flat or convex terrain (with greater spread due to more diverging flow). Once the areas potentially affected by a lahar are delineated, a probability function  $P_q$  assigns a relative probability of being affected by the lahar to each grid cell ( $i$ ). The probability is described by the function  $F_r$ , indicating that the more the flow diverts from the steepest descent direction the greater is the resistance.  $F_r$  yields a cell value which increases down valley from the location of initiation (increasing distance) and laterally at an angle of  $45^\circ$  from the steepest descent flow path (increasing flow resistance). The ratio between  $F_r$  and the horizontal distance  $H$  from each cell ( $i$ ) to the starting zone represents a probability function value (Huggel et al., 2003), and each cell value has a probability for being affected by the lahar:

$$P_q(i) = H(i)/F_r(i) \quad (1)$$

$P_q(i)$  is not a mathematical probability in a strict sense but depicts a qualitative probability.

### 3.2.2. Runout component of model

The runout component of the model defines an  $H/L$  ratio and hence the stopping conditions for the trajectory part. The  $H/L$  ratio is the slope between the initiation point of the lahar and the lowest deposition point. Unlike LAHARZ, the MSF model provides the potential inundation zones of a maximum lahar event including the probability-related values, indicating areas more or less likely to be affected. Consequently, the runout distance should also be based on a maximum extent. Minimum values of  $H/L$  ratios for lahars in combination with debris avalanches (corresponding to a maximum runout distance) based on empirical data have been proposed and range from about  $<0.02$  to  $0.1$  (e.g. Crandell, 1989; Siebert, 1996; Scott et al., 2001). However, for lahars the definition of a minimum  $H/L$  ratio is considerably complicated by processes such as flow transformation. Volcanic debris avalanches may transform into debris flows and eventually into hyperconcentrated streamflows (Pierson and Scott, 1985; Scott et al., 2001).

Definition of an  $H/L$  ratio based on a volume versus  $H/L$  relationship as it was presented for granular debris flows (e.g. Rickenmann, 1999) is difficult in view of flow transformation and debris-mobilization processes (bulking) along the flow path but can be feasible if sufficient reference data are available (cf. Fig. 3).

The approach applied here follows the reasoning behind a volume– $H/L$  relationship but is more practically motivated than strictly physically justifiable. In consideration of observed lahars at Popocatepetl attaining an  $H/L$  ratio of  $0.15$  with a volume of roughly  $1 \times 10^6 \text{ m}^3$ , a reasonable approximation for a probable maximum lahar of up to  $1 \times 10^7 \text{ m}^3$  (cf. Section 4) is  $0.10$ . The use of the  $H/L$  ratio suggesting a clear distinction between endangered and safe areas is not fully satisfactory and has been questioned earlier (Scott et al., 2001). We therefore emphasize the importance of not interpreting the model results as strict boundaries but rather as an approximate indication between endangered and safe areas. The probability-related

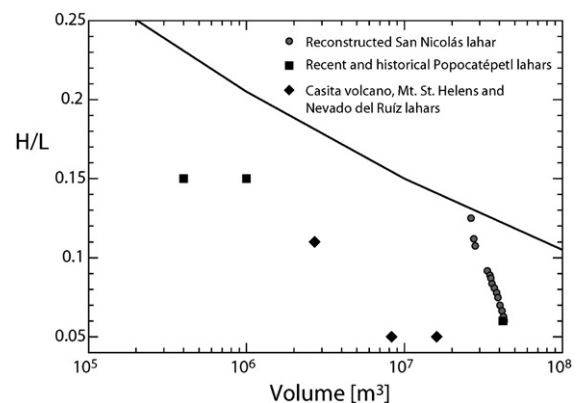


Fig. 3. Relation between fall height ( $H$ ) to runout length ( $L$ ) and lahar volume. The Popocatepetl lahars comprise the 2001, 1997 and the 1300 years B.P. events. The data points of the San Nicolás lahar 1300 years B.P. are based on reconstructed cross-sections and refer to volume estimates by González Huesca (2000). The relationship shown as a straight line is a transformation of an empirical equation by Rickenmann (1999) that relates  $L$  with  $V$  and  $H$ , derived from alpine-type, granular debris flows. Data for Mount St. Helens, Nevado del Ruiz and Casita Volcano are from Pierson and Janda (1994) and Scott et al. (2005).

representation of potential inundation areas of the MSF model provides a certain confidence value of lahar-affected areas.

## 4. Lahar modeling

### 4.1. Lahars at Popocatepetl

Since December 1994, when Popocatepetl Volcano began a new eruptive cycle, several lahars have occurred. The most remarkable ones took place in 1995, 1997 and 2001 along the Huiloac gorge and its tributaries, extending downstream to the town of Santiago Xalizintla (Sheridan et al., 2001; Capra et al., 2004). These lahars all occurred in connection with eruptive activity and related melting of Ventorrillo glacier (González Huesca and Delgado Granados, 1997).

The July 1, 1997, lahar showed a lag time between the pyroclastic flows and lahar initiation of 24 h (Oropeza Villalobos et al., 1999; Palacios et al., 2001). Although not known in detail, trigger mechanisms such as saturation of sediment due to melting of snow and ice have been suggested, reinforced by partly impermeable ground layers due to permafrost or ice-core occurrence, and the formation and release of subglacial water reservoirs (González Huesca and Delgado Granados, 1997; Oropeza Villalobos, 2001; Palacios et al., 2001). The July 1, 1997, lahar was non-cohesive and transformed into a hyperconcentrated streamflow further downstream (Capra et al., 2004). The sediment volume was estimated between  $330,000$  and  $400,000 \text{ m}^3$  with a sediment content of about 25% (Sheridan et al., 2001; Capra et al., 2004).

The January 21, 2001 lahar was also preceded by eruptive activity and pyroclastic flows but did not transform into a hyperconcentrated streamflow. The amount of water involved was significantly smaller than that in 1997, and the sediment volume was about  $240,000 \text{ m}^3$  with a sediment concentration of ca. 60% (Julio Miranda et al., 2005). The sediment primarily



originated from water-saturated pumice-flow deposits. Both the 1997 and the 2001 lahars reached the vicinity of Santiago Xalitziintla, 15 km from the source zone and 17 km from the vent. The lahars caused damage to agricultural land and other private property.

Evidence of much larger prehistoric lahars on the order of  $5 \times 10^7 \text{ m}^3$  was found in the Huiloac gorge extending down to the town of San Nicolás de los Ranchos and dating from 1100 to 1300 years before present (Siebe et al., 1996). González Huesca et al. (1997) and González Huesca (2000) described an event known as the San Nicolás lahar which almost reached the town of Izúcar de Matamoros, traveling nearly 60 km along the stream 1300 years ago.

The northwestern drainage area of Popocatepetl with the Nexpayantla gorge directed to the town of San Pedro Nexapa and other villages was barely affected by lahars during the new eruptive phase of Popocatepetl. The absence of ice-melting-related lahars at Nexpayantla gorge is because the drainage system of the Ventorrillo and Noroccidental glaciers is towards the Huiloac and Guadalupe gorges and not to Nexpayantla. Sheridan et al. (2001) reported on a prehistoric lahar extending far beyond San Pedro Nexapa with an estimated volume of  $1.2 \times 10^8 \text{ m}^3$  about 1100 to 1300 years ago when ice presumably still existed in the uppermost part of the Nexpayantla gorge or intense rainfall provided water for their formation.

#### 4.2. LAHARZ for Popocatepetl DEMs

Modeling of lahars using LAHARZ was applied to the Huiloac and Nexpayantla gorges. Determination of the modeled lahar volumes is a key parameter of the model setup. For the Huiloac drainage, the chosen lahar volumes were based on the 1995–2001 events, the available volume of water due to potential melting of

glacier ice and snow, and the historical record of lahars under conditions similar to the present. Due to strong glacier retreat in recent years (Huggel and Delgado, 2000; Julio Miranda and Delgado Granados, 2003), the water equivalent of ice has significantly decreased to about  $2.8 \times 10^6 \text{ m}^3$  at present. In accordance with studies on sedimentological characteristics of recent lahars in the Huiloac gorge (Capra et al., 2004; Julio Miranda et al., 2005) and more general flow-type considerations (e.g., Pierson and Scott, 1985; Pierson and Costa, 1987; Hungr et al., 2001), a sediment concentration of 25 to 65% is assumed for potential lahars and hyperconcentrated flows. Hence, given the maximum water volume available from melting processes, a maximum flow volume of  $3.7 \times 10^6 \text{ m}^3$  to  $8 \times 10^6 \text{ m}^3$  results. Determination of the  $H/L$  ratio for distinction of the upstream boundary of the distal hazard zone was based on sedimentological evidence of recent lahars (i.e. the onset of sediment deposition; Capra et al., 2004; Julio Miranda et al., 2005) and set to 0.32.

For the Nexpayantla gorge, less geological evidence exists for reconstructing potential lahar volumes. A likely scenario is lahar generation from rock avalanches or pyroclastic flows combined with very heavy rain. The modeled lahar volumes were chosen as  $5 \times 10^4 \text{ m}^3$ ,  $1 \times 10^5 \text{ m}^3$ ,  $5 \times 10^5 \text{ m}^3$  and  $3 \times 10^6 \text{ m}^3$  based on sediment volumes potentially available for flow mobilization. Very large events in the order of  $10^7 \text{ m}^3$  to  $10^8 \text{ m}^3$  were considered as having very low probability of occurrence but were included here to analyze the replication of the lahar 1100–1300 years ago (Sheridan et al., 2001) by the LAHARZ model.

Processing steps of the LAHARZ program, such as calculation of the energy cone, streamflows, or lahar cross sections, were found to be more stable with the SRTM DEM than with the ASTER DEM. Some of the processing steps have occasionally failed with the ASTER DEM, which is likely due to interpolated areas of missing data or errors in the drainage channels. The

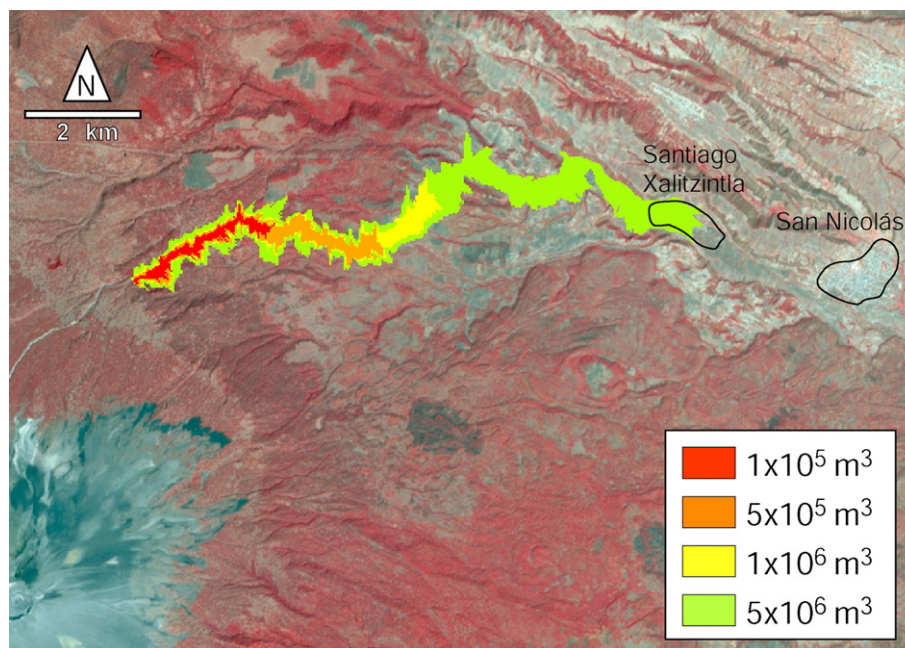


Fig. 4. Modeled lahars in the Huiloac gorge using LAHARZ and the ASTER DEM with four different lahar volumes. Base image is an ASTER near-infrared image where vegetation is shown in red colors (taken on 21 March 2001). Popocatepetl Volcano with the crater is visible in the lower left corner.

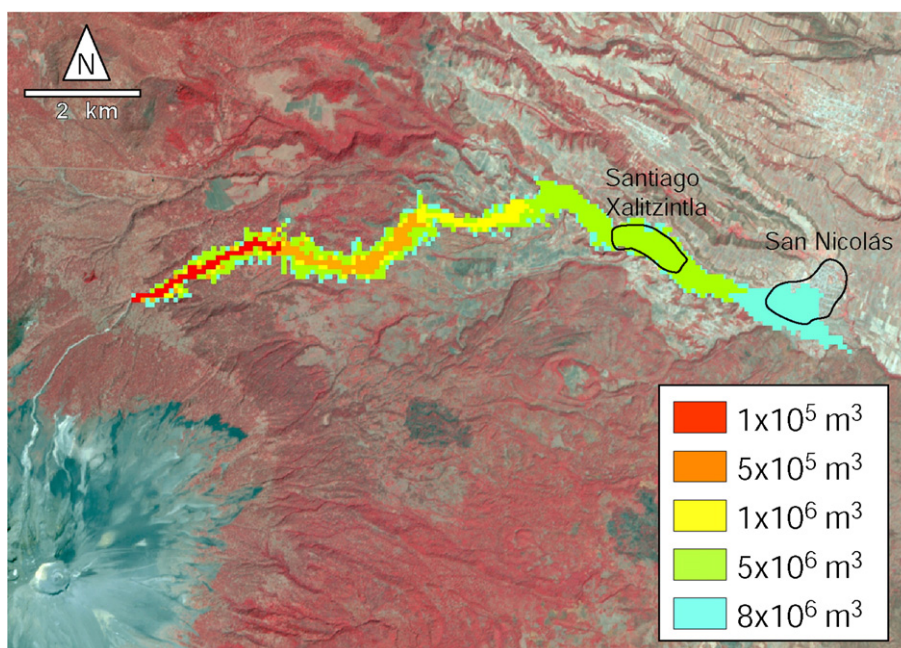


Fig. 5. Modeled lahars in the Huiloac gorge using LAHARZ and the SRTM DEM with five different lahar volumes. Base image is the same as Fig. 4. Note the difference in travel distance of the predicted lahars of equal volume in relation with those shown in Fig. 4.

results of model runs for the Huiloac gorge based on the ASTER-derived DEM show that only lahars with a volume of  $5 \times 10^6 \text{ m}^3$  or larger would reach the town of Santiago Xalitzintla (Fig. 4). Lahars modeled with the same flow volume but with SRTM terrain data (Fig. 5) travel 1.8 km further downstream passing Santiago Xalitzintla and almost reaching San Nicolás. As can be inferred from Fig. 4, the ASTER-based model tends to a stronger lateral distribution of the flow volume, thus limiting the longitudinal distribution (i.e. travel distance). In comparison to the observed lahar of corresponding volume in 1997, the modeled lahars fall short in travel distance by approximately 2 km and 4 km for SRTM and ASTER, respectively. The flow paths for the ASTER and SRTM DEMs are consistent except for the middle section where an erroneous flow-routing of the ASTER model can be observed, caused by an error of that DEM. In terms of total inundation area, results for the ASTER and SRTM-based Huiloac lahars differ as little as 2% (Table 1).

LAHARZ models for the Nexpayantla gorge show that lahars with a volume equal or larger than about  $5 \times 10^5 \text{ m}^3$  may represent

a hazard for the town of San Pedro Nexapa (Fig. 6). Due to a lack of recent lahar events, no detailed geological record exists here to relate modeled and observed inundation areas. The simulation of the historical  $1 \times 10^8 \text{ m}^3$  lahar yields a stronger confinement to the flow channel, and a stronger deviation to the south than indicated by the mapped deposits (Sheridan et al., 2001). In any case, and not surprisingly, a lahar of such a dimension, though very unlikely, would have a disastrous impact on today's populated areas.

#### 4.3. MSF for Popocatepetl DEMs

The MSF model was applied to the Huiloac and Nexpayantla gorges using ASTER and SRTM DEM data. Significant insight into the characteristics of the model in combination with the DEMs could thus be achieved. Unlike LAHARZ, no processing failure was recorded with the ASTER DEM (nor with the SRTM DEM) when running the MSF model.

For the Huiloac lahar, the starting location for the model was set at the head of the proglacial tributaries of the Huiloac gorge at 4700 m a.s.l. The lahars observed in recent years all had their origin in this zone immediately downstream of Ventorillo glacier, triggered by mobilization of ash, rock and ice avalanche deposits in connection with high melt-water input (Palacios et al., 2001). The initiation zone for the Nexpayantla drainage was defined at 4200 m a.s.l. at the toe of a major rockfall area at Cerro del Fraile, a remnant of a magmatic intrusion at Popocatepetl Volcano. Lahars can be triggered there by rainfall-induced mobilization of ash and rock deposits, or by transformation of a rock avalanche into a lahar. In consideration of the erodible sediment volume available, it may be assumed that lahars with a volume larger than about  $1 \times 10^6 \text{ m}^3$  would only occur in combination with a major rock avalanche. The lahar starting zones defined for the MSF model are different from those for LAHARZ. This is because of

Table 1  
Lahar-affected areas as calculated by the MSF and LAHARZ models based on SRTM and ASTER DEMs

	SRTM		ASTER		
	Amecameca	Huiloac	Huiloac		
MSF (km <sup>2</sup> )	36.52	29.13	30.63		
LAHARZ (m <sup>3</sup> , km <sup>2</sup> )	$1 \times 10^5$	$1 \times 10^5$	0.43	$1 \times 10^5$	0.44
	$3 \times 10^6$	$1 \times 10^6$	2.03	$1 \times 10^6$	2.01
	$1 \times 10^8$	$5 \times 10^6$	5.84	$5 \times 10^6$	5.85

For LAHARZ, inundation areas are given in relation to corresponding lahar volumes. Note that for the Huiloac gorge the MSF and LAHARZ models cannot be compared against each other because the modeled flow initiation point is different.



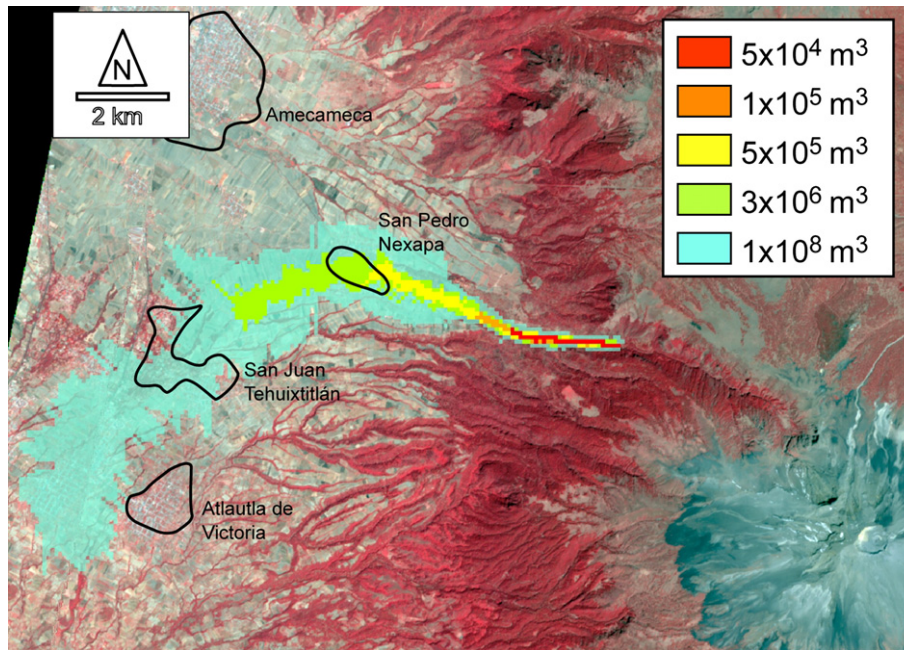


Fig. 6. Modeled lahars in the Nexpayantla gorge using LAHARZ and the SRTM DEM. The largest simulated lahar (light blue) replicates a prehistoric event 1100 to 1300 years B. P. (Sheridan et al., 2001).

the MSF model concept, which simulates the lahar from the initiation zone to predict an appropriate  $H/L$  ratio over the entire flow path. For comparison with modeling results from LAHARZ, tests were performed with the MSF model starting at the same location as with LAHARZ. Results did not show any significant difference of the shape of downstream inundated areas for different initiation zones defined for the MSF model.

For both drainages, the  $H/L$  ratio for confining the lahar runout is defined as 0.1. Beyond the basic controversy of constraining a lahar by definition of a  $H/L$  ratio, the value of 0.1 is reasonable in

view of the  $H/L$  ratio of 0.15 attained by recent lahars. The MSF model simulates reasonable maximum events which are defined here about half to one order of magnitude larger than the recent lahar events.  $H/L$  equal to 0.1 is thus supposed to realistically confine the lahar even though a physical basis for doing so is lacking.

The MSF model characteristically identifies different potential flow paths assigning a corresponding qualitative probability. In case of the Huiloac lahar, the MSF model indicates a possible flow deviation at about 3700 m a.s.l. with both the ASTER and

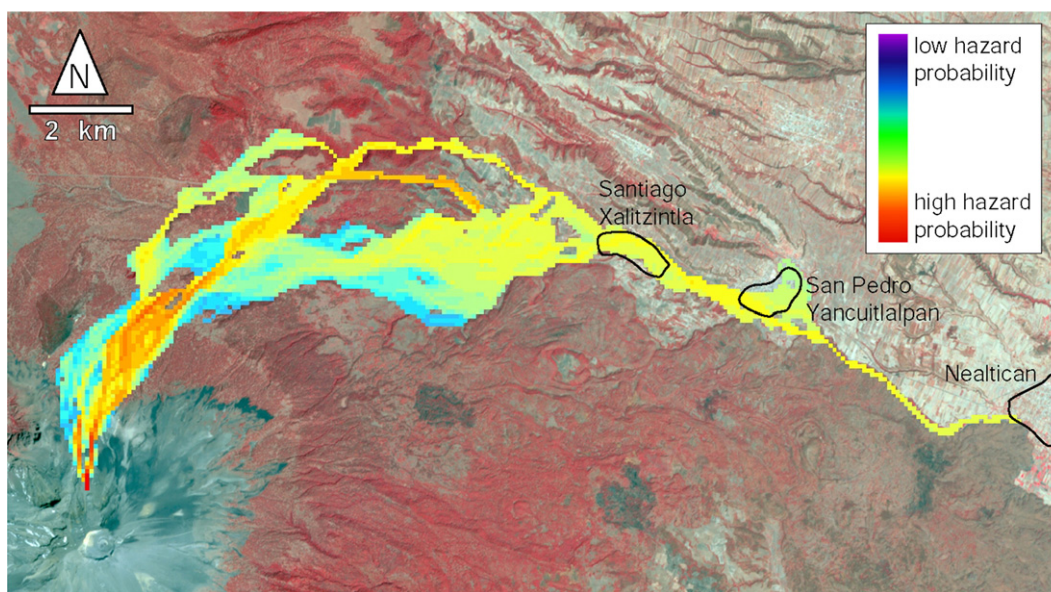


Fig. 7. MSF model simulating a probable maximum lahar event in the Huiloac gorge using the SRTM DEM. The runout is constrained by a  $H/L$  ratio of 0.1. Color coding refers to different degrees of probability for a cell to be affected by the lahar. The initiation zone of the lahar is defined at a higher elevation than in the LAHARZ model due to the MSF model concept (see text).



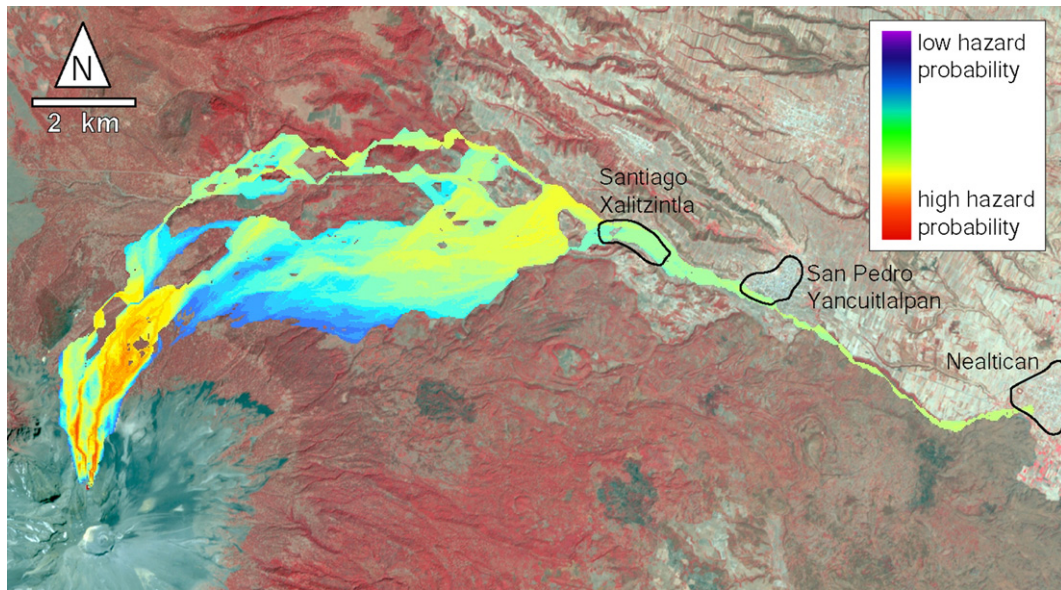


Fig. 8. MSF model simulating a probable maximum lahar event in the Huiloac gorge using the ASTER DEM. The runout is constrained by a  $H/L$  ratio of 0.1. Color coding refers to different degrees of probability for a cell to be affected by the lahar.

SRTM DEMs (Figs. 7 and 8). Verification of the field conditions at this point reveals a poorly defined flow channel, which would enable overflow in the model. The different flow paths join again about 3 km upstream from Santiago Xalitziintla. By using a  $H/L$  of 0.1, the simulated lahars just reach the town of Nealticán, 10 km downstream from Santiago Xalitziintla. There is a high correspondence of the simulated lahars when using the ASTER and the SRTM DEM. Except for the middle section, where the ASTER-based model shows a somewhat stronger lateral flow distribution, the potential inundation areas are much alike. In quantitative terms, the total inundation areas using the ASTER

and SRTM DEMs show a difference  $<5\%$  (Table 1). The modeled flow path between Santiago Xalitziintla and San Nicolás is characterized by confined channel flow in both DEM applications. This is evidence that the ASTER as well as the SRTM DEM adequately represent the channel topography. The color range of the models allows more and less likely affected areas to be distinguished.

The lahar simulations in the Nexpayantla gorge reveal the effects of errors and related interpolation of the ASTER DEM on the flow-routing. In the middle section of the gorge, the simulated lahar is diverted into the drainage channel to north (not

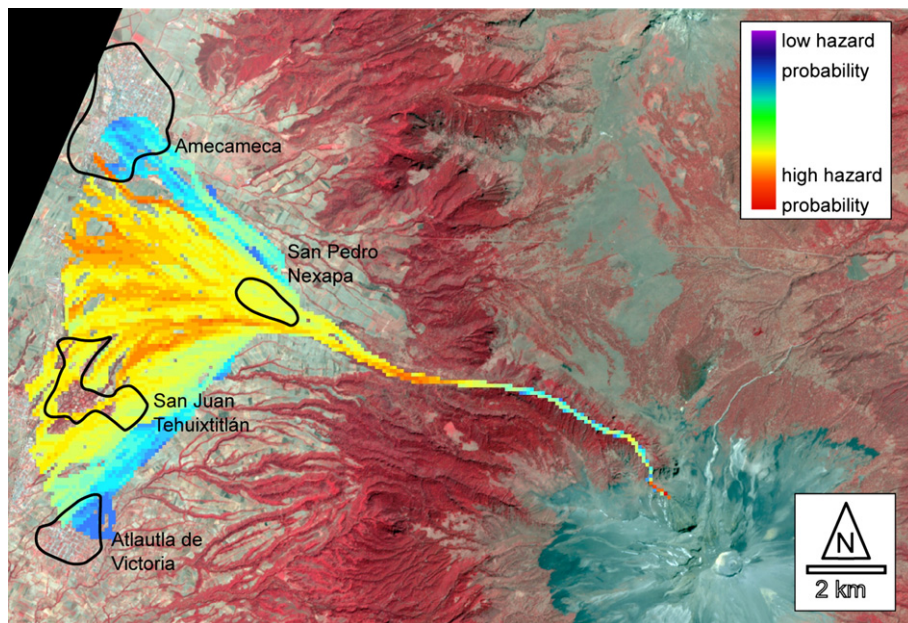


Fig. 9. MSF model simulating a probable maximum lahar event in the Nexpayantla gorge using the SRTM DEM. The runout is constrained by a  $H/L$  ratio of 0.1. Color coding refers to different degrees of probability for a cell to be affected by the lahar. The initiation zone of the lahar is defined at a higher elevation than in the LAHARZ model due to the MSF model concept (see text).

shown in figure). Such errors in the DEM should be recognized during the DEM analysis in order to avoid mis-interpretations.

The SRTM-based lahar model of the Nexpayantla gorge is first confined to the drainage channel and then defines flow spreading at the fan apex (Fig. 9). The model indicates a large inundated area, which is only realistic with a flow volume significantly larger than  $10^5 \text{ m}^3$  to  $10^6 \text{ m}^3$ . The geological record of the San Pedro lahar 1100 to 1300 years ago and the related areas affected (Sheridan et al., 2001) are reasonably consistent with the modeled inundation areas. According to the volume of the San Pedro lahar, the volume of the modeled lahar event may thus be inferred to be on the order of  $10^8 \text{ m}^3$ . It is notable that the MSF model also simulates a likely north-bound inundation area in addition to the south-bound area of LAHARZ.

## 5. Discussion

For the LAHARZ simulations, the model parameters were kept identical for both the ASTER and SRTM DEM. Hence, the difference in the modeling results, in particular the inundation areas and the travel distance, as observed for the Huiloac lahars, can be directly related to the DEMs used. The digital representation of the drainage channel and valley cross-section of each DEM determines the lateral distribution of the flow volume in LAHARZ; as a consequence, the travel distance and the delineation of the distal hazard zone are similarly determined. It is notable that the 90 m-SRTM DEM confines the lahar more strongly to the flow channel than the 30 m-ASTER DEM. Stronger lateral flow confinement of lower-resolution DEMs could be due to scaling phenomena. Scaling phenomena present with LAHARZ in connection with the lateral flow distribution and the shape of the inundated area was, in fact, already pointed out by Iverson et al. (1998) though they did not compare different DEM applications. The effect of scaling may not be straightforward and model response complex (Hardy et al., 1999). For instance, higher resolution of generically identical DEMs does not necessarily improve modeling results, as Horritt and Bates (2001) showed using a hydraulic raster-based flow-routing model. Stevens et al. (2002) investigated the effects of grid-spacing on lahar inundation zones predicted by LAHARZ by comparing a 10 m-gridded DEM with resampled derivatives of 30 m and 90 m resolution. No significant effect could be detected except for some lahars falling short in travel distance by 1–2 km when using the coarser spaced grids. The same feature (i.e., wider lateral spread and shorter longitudinal extent of coarser spaced grids) was also found for generically different DEMs of 25 m and 10 m resolution. This represents the opposite phenomenon of what was observed in the present study. Stevens et al. (2002) furthermore showed that the generic DEM type is responsible for a larger difference in LAHARZ modeling results than scaling phenomena, a finding which is consistent with our study. We thus argue that the more accurate representation of the main drainage channels by the SRTM DEM, and in general the generic type of the DEM, is a more critical issue influencing the model result. Despite the higher resolution, the ASTER DEM contains more vertical errors than the SRTM DEM. A comparison of the shape of the inundated area of the ASTER and

SRTM DEM-based modeling reveals good correspondence. Thus, the ASTER-based model, though finer spaced, does not add any significantly new information to the SRTM-based model with respect to the shape of the inundated area. A quantitative evaluation of the inundation area also yields only minor differences (2–5%) between ASTER and SRTM DEMs for both the LAHARZ and MSF models. The ASTER-SRTM comparison of the LAHARZ modeling reveals, however, that the choice of the DEM can have important effects on the determination of the distal hazard zone and thus on hazard assessment and mapping (see also Stevens et al., 2002, for comparison of a map-derived and an airborne InSAR DEM in combination with LAHARZ). With otherwise identical model parameters, the modeling using the ASTER and SRTM DEMs shows a difference of 1.8 km of the horizontal travel distance for the  $5 \times 10^6 \text{ m}^3$  lahar, or a 15 to 20% difference in relation to the total travel distance. Determination of hazard zones in critical areas (i.e., populated areas) should thus not be based on one DEM alone without any sensitivity analysis, and integration of a further DEM from different source data helps determining the range of model uncertainty.

In comparison with the observed lahars, the model runs with both the ASTER and SRTM DEM show a stronger lateral flow volume distribution in LAHARZ. For instance, the roughly  $1 \times 10^6 \text{ m}^3$ -volume lahar (including sediment and water content) in 1997 reached the town of Santiago Xalitzintla, while the modeled lahar with the same volume does not. Unlike in the MSF model, the strong lateral flow volume distribution has a significant effect on the modeled travel distance of the lahar in LAHARZ but not on the total area inundated. The extent of the distal hazard zone is thus underestimated, an effect that has to be seriously considered for corresponding hazard mapping.

Although the MSF model integrates similar flow algorithms as LAHARZ and is also run within a GIS environment, it follows otherwise a different concept: the flow path is not directly related to the flow volume but the latter is indirectly indicated by a probability function showing more and less likely flow trajectories and distribution. A direct quantitative comparison of LAHARZ and MSF is difficult. For the Nexpayantla gorge the MSF model may be closest to the LAHARZ model with a  $10^8 \text{ m}^3$  lahar. The difference of the total inundated area of LAHARZ and MSF using the SRTM DEM is  $\sim 27\%$  (Table 1). The travel distance of the MSF model is constrained by the *H/L* approach. As outlined above, definition of an *H/L* ratio for a lahar insufficiently represents the processes observed in nature and bears several uncertainties (Scott et al., 2001, 2005). Fig. 3 represents a compilation of the *H/L* ratio in relation to lahar volume for recent and historic events at Popocatepetl, and for some of the few corresponding published data available. Rickenmann (1999) proposed an empirical relationship for *H* and volume *V* to *L* for alpine (granular) debris flows (Fig. 3). However, as the few data indicate, such a relationship is more problematic for lahar-type flows. While debris flows are often characterized by a flow stopping abruptly in less inclined terrain when the yield stress necessary for flow mobility is under-run, lahars may transform into hyperconcentrated streamflow and continue for several kilometers without a well-defined runout length (Pierson and Scott, 1985, O'Brien et al., 1993). Models simulating lahar runout



based on *H/L* values thus cannot provide a clear definition of 'safe' and 'unsafe' zones. Although in this study a maximum credible approach under present conditions was applied for the lahar runout length, it cannot be excluded that a channelized lahar flow would surpass the modeled runout length due to processes such as sediment bulking or flow transformation.

The MSF model is clearly less sensitive to flow channels represented in the DEM than LAHARZ and may simulate overflow where LAHARZ constrains the flow to the channel. The resulting flow distribution may appear too wide for a lahar. However, these results should be understood as representing a maximum distribution and as an indicator of possible alternative flow paths in the case of a large event. According to recent studies, the MSF model has also been found suitable for delineating areas affected by mass-movement processes less confined to flow channels, such as debris or rock avalanches (Noetzli et al., 2006).

In sum, this study has shown that both ASTER and SRTM DEMs are feasible for lahar modeling with either of the two models applied. This represents an important finding in view of the nearly global availability of ASTER and SRTM data. As far as ASTER is concerned, it is furthermore of relevance that the sensor is capable of taking repeat stereo images for DEM generation, theoretically at every satellite overpass if weather conditions permit. On active volcanoes, the topography may change frequently due to accumulation of eruptive products, and hence exert a significant influence on the flow paths of mass movements (Renschler, 2005). Outdated DEM data may thus yield erroneous modeling results. ASTER provides an invaluable tool to acquire a digital representation of the current topographic situation of volcanoes at low cost.

## 6. Conclusions

This study has evaluated DEMs derived from ASTER and SRTM remote-sensing data for lahar modeling. Both types of DEMs basically have been found feasible for application with the mass-flow models LAHARZ and MSF. Due to the global coverage of ASTER and SRTM data, this conclusion implies that lahar modeling studies are possible on virtually any volcano. This is of particular importance for volcanoes lacking DEM information. For volcanoes with available DEMs (e.g., map-derived), the ASTER and SRTM data can validate lahar modeling based on the present topography.

The SRTM data, although of coarser spatial resolution, has proven to represent the actual topography more reliably than the ASTER DEM, especially with regard to the flow channels. ASTER DEMs can have problems on steep north-facing slopes, and related errors can cause incorrect lahar modeling. The generation of DEMs from ASTER imagery furthermore requires a cloud-free satellite image (due to optical sensor characteristics), which can be problematic, for instance, in regions of the tropics with nearly constant cloud cover. Where adequate topographic and atmospheric conditions for DEM generation prevail, ASTER DEMs are able to provide considerable detail for lahar flow distribution. We furthermore found that the shape and the total extent of predicted inundated areas based on

ASTER and SRTM DEMs are fairly consistent. Significant differences in the modeled travel distance of lahars of the same volume, however, were revealed when using the 30 m-ASTER and the 90 m-SRTM DEMs with LAHARZ. This was due to stronger lateral flow distribution in the ASTER-based model. The generic type of DEM used, and not scaling phenomena, are primarily responsible for this effect.

In more general terms, we conclude that the type of DEM used is highly relevant for the results obtained with LAHARZ, a particularly important finding to consider when modeling results are used for hazards assessment and mapping. In practice, however, often there has not been any alternative option to the DEM available to date, if even a DEM was available at all. Nowadays, digital terrain data from the space-borne sensors ASTER and SRTM, or in some cases even from very-high-resolution sensors, such as QuickBird or SPOT-5, can improve results and reliability of lahar modeling. When only one DEM is available, our current study strongly suggests the need to analyze the accuracy and quality of the DEM with sensitivity tests prior to lahar modeling.

## Acknowledgements

This research was initiated during the sabbatical leave of Hugo Delgado at the University of Zurich under the sponsorship of Dirección General de Asuntos del Personal Académico (UNAM). Support and constructive comments on the manuscript by Wilfried Haerberli are greatly acknowledged. The paper much benefited from stimulating and constructive reviews by Bruce H. Raup and Kevin M. Scott.

## References

- Abrams, M., 2000. ASTER: Data products for the high spatial resolution imager on NASA's Terra platform. *Int. J. Remote Sens.* 21, 847–853.
- Brugman, M., Delgado Granados, H., 1998. Evaluating glacier-related hazards on an active volcano: Popocatepetl Volcano, Mexico City. *Geomatic in the era of Radarsat*, Ottawa, Ontario, Canada, June 9–11, 1998, pp. 276–277. Abstracts.
- Bursik, M., Martínez-Kackert, B., Delgado Granados, H., González Huesca, A., 2003. A smoothed-particle hydrodynamic automaton of landform degradation by overland flow. *Geomorphology* 53, 25–44.
- Capra, L., Poblete, M.A., Alvarado, R., 2004. The 1997 and 2001 lahars of Popocatepetl Volcano (Central Mexico): textural and sedimentological constraints on their origin and hazards. *J. Volcanol. Geotherm. Res.* 131, 351–369.
- Crandell, D.R., 1989. Gigantic debris avalanche of Pleistocene age from Mount Shasta Volcano, California, and debris-avalanche hazard zonation. *U.S. Geol. Surv. Bull.* 1861 29 pp.
- Delgado Granados, H., 1997. The glaciers of Popocatepetl Volcano, Mexico: changes and causes. *Quat. Int.* 43, 1–8.
- Delgado Granados, H., Brugman, M., 1995. Monitoreo de los glaciares del Popocatepetl. *Volcán Popocatepetl, Estudios Realizados durante la Crisis de 1994–1995*, CENAPRED-UNAM, pp. 221–244.
- Delgado Granados, H., Panfil, M., González Huesca, E.A., Uruñuela, G., Plunket, P., Gardner, T., Abrams, M., 1994. Lessons from Popocatepetl Volcano (Mexico): ancient settlement buried by lavas, mudflows, and air-fall deposits. *American Geophysical Union Annual Meeting 1994*, p. 737. Abstracts.
- Delgado Granados, H., González Huesca, E.A., Molinero, R., 1995. The San Nicolás Lahar at Popocatepetl Volcano (Mexico): blast triggered lahar involving melting of an ice mass. *Geological Society of America Annual Meeting New Orleans, Louisiana*, 6–10 November 1995. Abstracts, A-358-359.

- González Huesca, E.A., 2000. Estudios de detalle estratigráfico y sedimentológico del Lahar de San Nicolás en el flanco noreste del volcán Popocatepetl. Engineering thesis, UNAM, Mexico, 109 pp.
- González Huesca, A.E., Delgado Granados, H., Urrutia Fucugauchi, J., 1997. The San Nicolás Lahar at Popocatepetl Volcano (Mexico): a case study of a glacier-ice-melt-related debris flow, triggered by a blast at the onset of a plinian eruption. International Association of Volcanology and Chemistry of the Earth's Interior, General Assembly, Puerto Vallarta, Mexico, 19–24 January 1997, p. 94. Abstracts.
- González Huesca, E.A., Delgado Granados, H., 1997. Los eventos laháricos de junio de 1997 en el volcán Popocatepetl: ¿Eventos generados por Jökulhlups? Reunión Anual Unión Geofísica Mexicana, Puerto Vallarta, Jalisco, 3–7 November 1997, p. 269. Abstracts.
- Hardy, R.J., Bates, P.D., Anderson, M.G., 1999. The importance of spatial resolution in hydraulic models for floodplain environments. *J. Hydrol.* 216 (3–4), 124–136.
- Hirano, A., Welch, R., Lang, H., 2003. Mapping from ASTER stereo image data: DEM validation and accuracy assessment. *ISPRS J. Photogramm. Remote Sens.* 57 (5–6), 356–370.
- Horritt, M.S., Bates, P.D., 2001. Effects of spatial resolution on a raster based model of flood flow. *J. Hydrol.*, 253 (1–4), 239–249.
- Huggel, C., Delgado, H., 2000. Glacier monitoring at Popocatepetl Volcano, México: glacier shrinkage and possible causes. In: Hegg, C., Vonder Muehll, D. (Eds.), *Beiträge zur Geomorphologie.- Proceedings Fachtagung der Schweizerischen Geomorphologischen Gesellschaft*, 8–10 July 1999, Bramois, WSL Birmensdorf, pp. 97–106.
- Huggel, C., Kääb, A., Haeblerli, W., Krummenacher, B., 2003. Regional-scale GIS-models for assessment of hazards from glacier lake outbursts: evaluation and application in the Swiss Alps. *Nat. Hazards Earth Syst. Sci.* 3 (6), 647–662.
- Hung, O., Evans, S.G., Bovis, M., Hutchinson, J.N., 2001. Review of the classification of landslides of the flow type. *Environ. Eng. Geol.* 7 (3), 221–238.
- Iverson, R.M., Schilling, S.P., Vallance, J.W., 1998. Objective delineation of lahar-inundation hazard zones. *Geol. Soc. Amer. Bull.* 110, 972–984.
- Julio Miranda, P., Delgado Granados, H., 2003. Fast hazard evaluation, employing digital photogrammetry on Popocatepetl glaciers, Mexico. *Geofis. Int.* 42 (2), 275–283.
- Julio Miranda, P., González Huesca, A.E., Delgado Granados, H., Kääb, A., 2005. Ice-fire interactions at Popocatepetl Volcano (Mexico): case study of the January 22, 2001 eruption. *Z. Geomorphol.* 140, 93–102.
- Kääb, A., 2002. Monitoring high-mountain terrain deformation from air and spaceborne optical data: Examples using digital aerial imagery and ASTER data. *ISPRS J. Photogramm. and Remote Sens.* 57 (1–2), 39–52.
- Kääb, A., 2005. Combination of SRTM3 and repeat ASTER data for deriving alpine glacier flow velocities in the Bhutan Himalaya. *Remote Sens. Environ.* 94 (4), 463–474.
- Kääb, A., Wessels, R., Haeblerli, W., Huggel, C., Kargel, J.S., Khalsa, S.J.S., 2003. Rapid Aster imaging facilitates timely assessments of glacier hazards and disasters. *EOS, Trans. Am. Geophys. Union*, 13 (84), 117–121.
- Major, J.J., Newhall, C.G., 1989. Snow and ice perturbation during historical volcanic eruptions and the formation of lahars and floods. *Bull. Volcanol.* 52, 1–27.
- Malin, M.C., Sheridan, M.F., 1982. Computer-assisted mapping of pyroclastic surges. *Science* 217, 637–640.
- Noetzi, J., Huggel, C., Hoelzle, M., Haeblerli, W., 2006. GIS-based modelling of rock/ice avalanches from Alpine permafrost areas. *Comput. Geosci.* 10 (2), 161–178.
- O'Brien, J.S., Julien, P.Y., Fullerton, W.T., 1993. Two-dimensional water flood and mudflow simulation. *J. Hydraul. Eng.* 119 (2), 244–261.
- O'Callaghan, J.F., Mark, D.M., 1984. The extraction of drainage networks from digital elevation data. *Comput. Vis. Graph. Image Proc.* 28, 323–344.
- Oropeza Villalobos, B., 2001. Caracterización física de los flujos laháricos originados de enero de 1999 a octubre de 2000 en el sector NE del volcán Popocatepetl. Master thesis, Geophysical Institute, UNAM, Mexico, 92 pp.
- Oropeza Villalobos, B., Delgado Granados, H., Ruíz García, B., 1999. Análisis espectral de los datos de detectores de flujo del volcán Popocatepetl. Reporte preliminar. Simposio Internacional Volcán Popocatepetl, México D. F., 22–24 March 1999, p. 29.
- Palacios, D., Marcos, J., 1998. Glacial retreat and its geomorphologic effects on Mexico's active volcanoes, 1994–1995. *J. Glaciol.* 44 (146), 63–67.
- Palacios, D., Zamorano, J.J., Parrilla, G., 1998. Proglacial debris flows in Popocatepetl north face and their relation to 1995 eruption. *Z. Geomorph. N.F.* 42 (3), 273–295.
- Palacios, D., Zamorano, J.J., Gomez, A., 2001. The impact of present lahars on the geomorphologic evolution of proglacial gorges: Popocatepetl, Mexico. *Geomorphology* 37, 15–42.
- Pieri, D., Abrams, M., 2004. ASTER watches the world's volcanoes: a new paradigm for volcanological observations from orbit. *J. Volcanol. Geotherm. Res.* 135, 13–28.
- Pierson, T.C., Scott, K.M., 1985. Downstream dilution of a lahar: transition from debris flow to hyperconcentrated streamflow. *Water Resour. Res.* 21 (10), 1511–1524.
- Pierson, T.C., Costa, J.E., 1987. A rheologic classification of subaerial sediment-water flows. In: Costa, J.E., Wieczorek, G.F. (Eds.), *Debris Flows/Avalanches: Process, Recognition, and Mitigation*. *Geol. Soc. Am., Rev. Eng. Geol.*, vol. 7, pp. 1–12.
- Pierson, T.C., Janda, R.J., 1994. Volcanic mixed avalanches: a distinct eruption-triggered mass-flow process at snow-clad volcanoes. *Geol. Soc. Amer. Bull.* 106, 1351–1358.
- Rabus, B., Eineder, M., Roth, A., Bamler, R., 2003. The shuttle radar topography mission a new class of digital elevation models acquired by spaceborne radar. *ISPRS J. Photogramm. and Remote Sens.* 57 (4), 241–262.
- Renschler, C.S., 2005. Scale and uncertainties in using models and GIS for volcano hazard prediction. *J. Volcanol. Geotherm. Res.* 139, 1–21.
- Rickenmann, D., 1999. Empirical relationships for debris flows. *Nat. Hazards* 19, 47–77.
- Schilling, S.P., 1998. LAHARZ: GIS programs for automated mapping of lahar-inundation hazard zones. US Geological Survey Open-File Report, vol. 98-638. 79 pp.
- Scott, K.M., Macías, J.L., Naranja, J.A., Rodríguez, S., McGeehin, J.P., 2001. Catastrophic debris flows transformed from landslides in volcanic terrains: mobility, hazard assessment, and mitigation strategies. *U.S. Geol. Surv. Prof. Pap.*, vol. 1630. 59 pp.
- Scott, K.M., Vallance, J.W., Kerle, N., Macías, J.L., Strauch, W., Devoli, G., 2005. Catastrophic precipitation-triggered lahar at Casita volcano, Nicaragua: occurrence, bulking and transformation. *Earth Surf.* 30, 59–79.
- Sheridan, M.F., Hubbard, B., Bursik, M.I., Abrams, M., Siebe, C., Macías, J.L., Delgado, H., 2001. Gauging short-term volcanic hazards at Popocatepetl. *EOS, Trans. Am. Geophys. Union* 82, 185–188.
- Siebe, C., Abrams, M., Macías, J.L., Obenholzer, J., 1996. Repeated volcanic disasters in Prehispanic time at Popocatepetl, central Mexico: past key to the future? *Geology* 24, 399–402.
- Siebe, C., Schaaf, P., Urrutia-Fucugauchi, J., 1999. Mammoth bones embedded in a late Pleistocene lahar from Popocatepetl Volcano, near Tocuila, central Mexico. *Geol. Soc. Amer. Bull.* 111, 1550–1562.
- Siebert, L., 1996. Hazard of large volcanic debris avalanches and associated eruptive phenomena. In: Scarpa, R., Tilling, R.I. (Eds.), *Monitoring and Mitigation of Volcano Hazards*. Springer, Berlin, pp. 541–572.
- Stevens, N.F., Manville, V., Heron, D.W., 2002. The sensitivity of a volcanic flow model to digital elevation model accuracy: experiments with digitised map contours and interferometric SAR at Ruapehu and Taranaki volcanoes, New Zealand. *J. Volcanol. Geotherm. Res.* 119, 89–105.
- Stevens, N.F., Garbeil, H., Mouginiis-Mark, P.J., 2004. NASA EOS Terra ASTER: Volcanic topographic mapping and capability. *Remote Sens. Environ.* 90, 405–414.
- Sun, G., Ranson, K.J., Kharuk, V.I., Kovacs, K., 2003. Validation of surface height from Shuttle Radar Topography Mission using Shuttle laser altimeter. *Remote Sens. Environ.* 88 (4), 401–411.
- Thouret, J.-C., 1990. Effects of the November 13, 1985 eruption on the snow pack and ice cap of Nevado del Ruiz volcano, Colombia. *J. Volcanol. Geotherm. Res.* 41, 177–201.
- Toutin, T., Cheng, P., 2001. DEM generation with ASTER stereo data. *Earth Obs. Mag.* 10 (6), 10–13.
- Van Zyl, J.J., 2001. The Shuttle Radar Topography Mission (SRTM): a breakthrough in remote sensing of topography. *Act Astrona.* 48 (5–12), 559–565.